nature medicine

Inhibition of Notch signaling promotes browning of white adipose tissue and ameliorates obesity

Pengpeng Bi[1], Tizhong Shan[1], Weiyi Liu[1], Feng Yue[1], Xin Yang[1], Xin-Rong Liang[1], Jinghua Wang[1], Jie Li[2], Nadia Carlesso[3], Xiaoqi Liu[2,4] & Shihuan Kuang[1,4]

Beige adipocytes in white adipose tissue (WAT) are similar to classical brown adipocytes in that they can burn lipids to produce heat. Thus, an increase in beige adipocyte content in WAT browning would raise energy expenditure and reduce adiposity. Here we report that adipose-specific inactivation of *Notch1* or its signaling mediator *Rbpj* in mice results in browning of WAT and elevated expression of uncoupling protein 1 (Ucp1), a key regulator of thermogenesis. Consequently, as compared to wild-type mice, Notch mutants exhibit elevated energy expenditure, better glucose tolerance and improved insulin sensitivity and are more resistant to high fat diet–induced obesity. By contrast, adipose-specific activation of Notch1 leads to the opposite phenotypes. At the molecular level, constitutive activation of Notch signaling inhibits, whereas Notch inhibition induces, *Ppargc1a* and *Prdm16* transcription in white adipocytes. Notably, pharmacological inhibition of Notch signaling in obese mice ameliorates obesity, reduces blood glucose and increases Ucp1 expression in white fat. Therefore, Notch signaling may be therapeutically targeted to treat obesity and type 2 diabetes.

The global epidemic of obesity and its associated risks of chronic diseases, including type 2 diabetes, pose formidable challenges to human health. Classical brown adipose tissue (BAT) found prominently in rodents and hibernating mammals dissipates extra energy to generate heat through uncoupled respiration mediated by UCP1 and thus increases energy expenditure and counteracts obesity[1–4]. Metabolically active UCP1$^+$ brown adipocytes have been detected recently in adult humans with advanced imaging techniques[5–9]. Interestingly, human adipose depots are highly heterogeneous, and brown adipocytes coexist with white and beige (brown-in-white, or brite) adipocytes[10–12]. Beige adipocytes are a class of adaptive thermogenic cells located within various depots of WAT[13–17]. Recent studies have indicated that beige adipocyte homeostasis can be maintained through two mechanisms. First, they can be generated *de novo* from a population of beige preadipocytes[18,19]. Second, they can be bi-directionally converted from and to white adipocytes under the control of environmental temperature or sympathetic nerve innervation[20–22]. Elevated UCP1 expression in cold-acclimated beige adipocytes is associated with robust uncoupled respiration and thermogenesis[23]. Notably, the appearance of beige or brown adipocytes in humans is inversely correlated with obesity and type 2 diabetes mellitus[24,25], indicating the important role of these adipocytes in regulating metabolism. Thus, identifying the mechanisms underlying beige adipocyte biogenesis is instrumental in the development of therapeutics to reduce adiposity and the risk of obesity-related metabolic syndrome, which affects over 10% of the world population.

Notch signaling is activated by binding of Dll or Jag family ligands with Notch receptors (Notch1–Notch4), leading to γ-secretase–mediated proteolytic cleavage and the release of Notch intracellular domain (NICD)[26]. NICD then translocates to the nucleus, where it binds with the Rbpj transcriptional complex to activate the transcription of downstream targets, including Hes and Hey family genes. Paradoxically, Notch signaling has been shown to either inhibit or facilitate the adipogenic differentiation of 3T3-L1 cells[27–30]. In mouse and human primary cell cultures, Notch inhibition promotes, whereas Notch activation inhibits, adipogenic differentiation of mesenchymal and adipose-derived stem cells[31–33]. However, genetic ablation of several key components of the signaling pathway has indicated that Notch signaling is dispensable for the adipogenesis of mouse embryonic stem cells or embryonic fibroblasts derived from early embryos[34]. As these studies were conducted in cultured cells, the function of Notch signaling in adipose tissues *in vivo* remains unknown. Here we report that the Notch pathway inhibits browning of white adipose tissue and regulates body energy homeostasis *in vivo*. This finding opens a new avenue to understand the molecular control of adipose plasticity and develop therapeutics to treat the emerging epidemics of obesity and diabetes through inhibition of Notch signaling transduction.

RESULTS

White- to beige-fat transition in Notch-signaling mutant mice

We first examined the relative expression of Notch pathway genes in different depots of WAT from wild-type (WT) mice. Notably, the mRNA levels of *Notch* receptors and Notch targets were much higher in visceral epididymal WAT (EpiWAT) than in subcutaneous inguinal

[1]Department of Animal Sciences, Purdue University, West Lafayette, Indiana, USA. [2]Department of Biochemistry, Purdue University, West Lafayette, Indiana, USA. [3]Department of Pediatrics, Indiana University School of Medicine, Indianapolis, Indiana, USA. [4]Center for Cancer Research, Purdue University, West Lafayette, Indiana, USA. Correspondence should be addressed to S.K. (skuang@purdue.edu).

Received 7 April; accepted 28 May; published online 20 July 2014; doi:10.1038/nm.3615

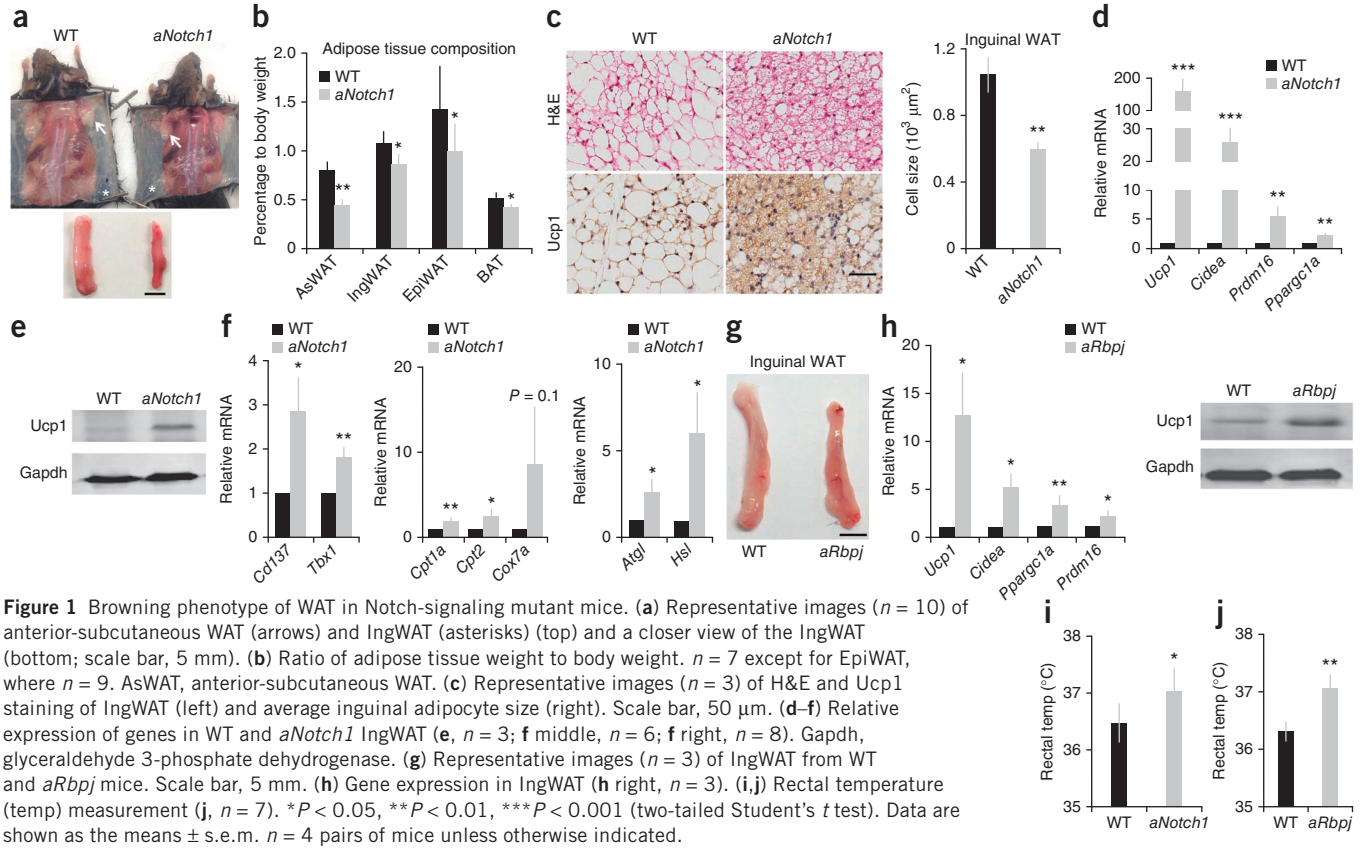

Figure 1 Browning phenotype of WAT in Notch-signaling mutant mice. (**a**) Representative images ($n = 10$) of anterior-subcutaneous WAT (arrows) and IngWAT (asterisks) (top) and a closer view of the IngWAT (bottom; scale bar, 5 mm). (**b**) Ratio of adipose tissue weight to body weight. $n = 7$ except for EpiWAT, where $n = 9$. AsWAT, anterior-subcutaneous WAT. (**c**) Representative images ($n = 3$) of H&E and Ucp1 staining of IngWAT (left) and average inguinal adipocyte size (right). Scale bar, 50 μm. (**d**–**f**) Relative expression of genes in WT and *aNotch1* IngWAT (**e**, $n = 3$; **f** middle, $n = 6$; **f** right, $n = 8$). Gapdh, glyceraldehyde 3-phosphate dehydrogenase. (**g**) Representative images ($n = 3$) of IngWAT from WT and *aRbpj* mice. Scale bar, 5 mm. (**h**) Gene expression in IngWAT (**h** right, $n = 3$). (**i**,**j**) Rectal temperature (temp) measurement (**j**, $n = 7$). $^*P < 0.05$, $^{**}P < 0.01$, $^{***}P < 0.001$ (two-tailed Student's *t* test). Data are shown as the means ± s.e.m. $n = 4$ pairs of mice unless otherwise indicated.

WAT (IngWAT) (**Supplementary Fig. 1a**,**b**). By contrast, the BAT-specific genes *Ucp1*, *Ppargc1a* and *Prdm16* were expressed at lower levels in EpiWAT than in IngWAT (**Supplementary Fig. 1c**). We also observed an inverse correlation between activated Notch1 (N1ICD) and Ucp1 at the protein level (**Supplementary Fig. 1d**). These results suggest that Notch signaling may have a role in regulating BAT-specific gene expression *in vivo*.

To directly investigate how Notch signaling regulates adipose plasticity *in vivo*, we established an adipose-specific *Notch1* knockout mouse model: *aP2-cre/Notch1*$^{flox/flox}$, henceforth referred to as *aNotch1*. To validate the tissue specificity of *aP2-cre*, we evaluated YFP fluorescence in different organs of *aP2-cre/Rosa*^{eYFP} reporter mice. As expected, all adipocytes were YFP$^+$, but liver and muscle tissues, two important regulators of lipid and glucose homeostasis, were predominately YFP$^-$ with only a few YFP$^+$ interstitial cells (**Supplementary Fig. 2a**). Adipose macrophages, accounting for <2% of the total stromal vascular fraction (SVF) cells, were also predominantly YFP$^-$ (**Supplementary Fig. 2b**,**c**). PCR-based genotyping confirmed DNA recombination in the adipose tissues of *aNotch1* mice (**Supplementary Fig. 2d**). Accordingly, *Notch1* expression was ~65% lower in adipose tissues and 85% lower in mature adipocytes but was unchanged in other tissues of *aNotch1* mice compared to WT mice (**Supplementary Fig. 2e**). Notably, various depots of subcutaneous WAT of *aNotch1* mice appeared browner than their WT counterparts (**Fig. 1a**). In addition, the weight of various fat depots was lighter in *aNotch1* compared to WT mice (**Fig. 1b**). Furthermore, multilocular Ucp1$^+$ beige adipocytes were much more abundant in the IngWAT of *aNotch1* compared to WT mice (**Fig. 1c**). The average adipocyte sizes of WAT in *aNotch1* mice were ~40% smaller than those in WT mice (**Fig. 1c**). At the molecular level, the expression of *Ucp1*, *Cidea*, *Prdm16* and *Ppargc1a* was higher in the IngWAT of *aNotch1* compared to WT mice (**Fig. 1d**). Western blot analysis confirmed the higher Ucp1 protein levels in the IngWAT of *aNotch1* mice compared to WT mice (**Fig. 1e**). In addition, mRNA levels of beige cell markers (*Cd137*, also called *Tnfrsf9*, and *Tbx1*), mitochondria genes (*Cpt1a* and *Cpt2*) and lipolysis enzymes (*Atgl*, also called *Pnpla2*, and *Hsl*, also called *Lipe*) were all considerably higher in the IngWAT of *aNotch1* mice than WT mice (**Fig. 1f**). We observed similar browning phenotypes in visceral EpiWAT but not BAT of *aNotch1* mutant mice (**Supplementary Fig. 2f–h**).

In parallel we generated another mouse model, *aP2-cre/Rbpj*$^{flox/flox}$ (*aRbpj*). Genotyping and quantitative PCR (qPCR) confirmed deletion of *Rbpj* DNA and lower expression levels of *Rbpj* mRNA in adipose tissues of *aRbpj* as compared to WT mice (**Supplementary Fig. 2d**,**i**). We again observed a browner appearance of IngWAT in *aRbpj* compared to WT mice (**Fig. 1g**), which was associated with higher expression levels of BAT-specific genes (**Fig. 1h**). However, expression of these genes was not altered in the BAT (**Supplementary Fig. 2i**). Of note, the *aNotch1* and *aRbpj* mice both had higher rectal temperatures than their WT siblings (**Fig. 1i**,**j**), indicating that the higher Ucp1 expression levels result in elevated thermogenesis *in vivo*.

Improved glucose metabolism in Notch-signaling mutant mice

In rodents and humans, brown adipocytes have been shown to improve glucose metabolism and insulin sensitivity[35,36]. To check whether browning of WAT in *aNotch1* mice elicits beneficial metabolic effects, we conducted intraperitoneal glucose- and insulin-tolerance tests (IP-GTT and IP-ITT, respectively). Compared to their WT siblings, *aNotch1* mice had lower blood glucose concentrations after glucose or insulin injection (**Fig. 2a**,**b**). We further measured

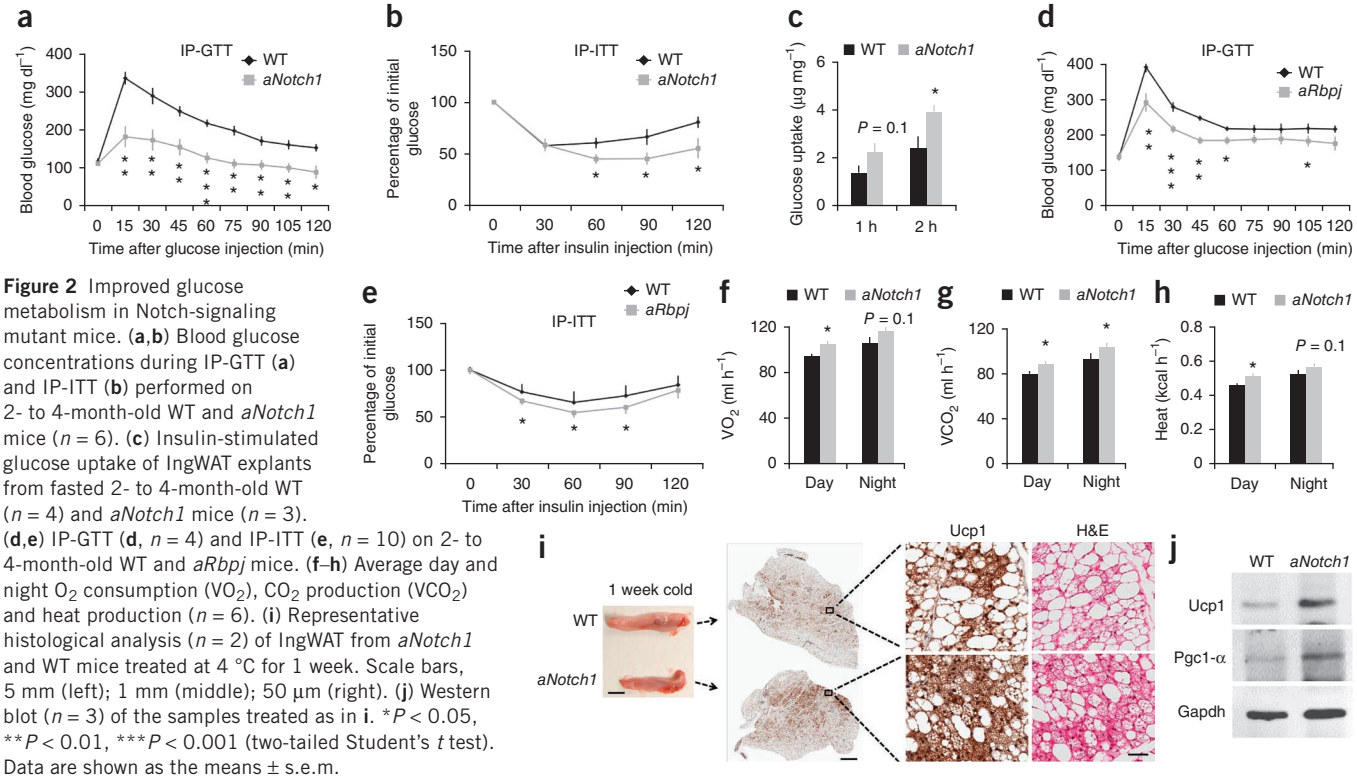

Figure 2 Improved glucose metabolism in Notch-signaling mutant mice. (**a**,**b**) Blood glucose concentrations during IP-GTT (**a**) and IP-ITT (**b**) performed on 2- to 4-month-old WT and *aNotch1* mice ($n = 6$). (**c**) Insulin-stimulated glucose uptake of IngWAT explants from fasted 2- to 4-month-old WT ($n = 4$) and *aNotch1* mice ($n = 3$). (**d**,**e**) IP-GTT (**d**, $n = 4$) and IP-ITT (**e**, $n = 10$) on 2- to 4-month-old WT and *aRbpj* mice. (**f**–**h**) Average day and night O_2 consumption (VO_2), CO_2 production (VCO_2) and heat production ($n = 6$). (**i**) Representative histological analysis ($n = 2$) of IngWAT from *aNotch1* and WT mice treated at 4 °C for 1 week. Scale bars, 5 mm (left); 1 mm (middle); 50 μm (right). (**j**) Western blot ($n = 3$) of the samples treated as in **i**. $^*P < 0.05$, $^{**}P < 0.01$, $^{***}P < 0.001$ (two-tailed Student's *t* test). Data are shown as the means ± s.e.m.

insulin-stimulated glucose uptake by IngWAT explants and found that IngWAT from *aNotch1* mice absorbed ~65% more glucose than that from WT mice (**Fig. 2c**). We also observed improved glucose tolerance and insulin-stimulated glucose clearance in *aRbpj* compared to WT mice (**Fig. 2d**,**e**). These *in vivo* and *ex vivo* experiments together suggest that genetic disruption of Notch signaling in adipose tissue improves insulin sensitivity and blood glucose tolerance.

A physiological characteristic of beige cells is their highly active metabolism coupled to thermogenesis. We examined the metabolic rate of *aNotch1* mice using an indirect calorimetry approach. *aNotch1* mice had higher rates of oxygen (O_2) consumption and carbon dioxide (CO_2) production and expended more energy than WT mice despite similar motor behaviors (**Fig. 2f–h** and **Supplementary Video 1**). To examine whether the metabolic changes were dependent on Ucp1 function, we acclimated mice at thermoneutral conditions (28.3 °C) for 3–5 weeks to block the functional activation of Ucp1. Notably, thermoneutrality abolished the beneficial metabolic phenotypes of the *aNotch1* mice observed at room temperature but not Ucp1 protein expression (**Supplementary Fig. 3**). This result suggests that the browning of WAT in *aNotch1* mice leads to Ucp1-dependent improvements of energy expenditure.

Contrary to thermoneutrality, cold stress induces the formation of beige adipocytes and their adaptive thermogenesis through UCP1 upregulation and sympathetic nerve stimulation[37]. Notably, IngWAT of *aNotch1* mice contained many more clusters of $Ucp1^+$ cells than IngWAT from WT mice after exposure to 4 °C for 1 week (**Fig. 2i**). In addition, adipocytes in the IngWAT from *aNotch1* mice were predominantly multilocular and $Ucp1^+$, whereas that from WT mice only contained a small fraction of such cells (**Fig. 2i**). These morphological changes were associated with elevated expression of Ucp1 and Pgc1-α (encoded by *Ppargc1a*) in IngWAT from cold-acclimated *aNotch1* mice compared to that from WT mice under similar conditions (**Fig. 2j**). These results indicate that *aNotch1* mice are more adaptive than WT mice to cold-induced thermogenesis.

The *aNotch1* mice are resistant to high fat diet–induced obesity

In light of their better glucose tolerance, insulin sensitivity and higher metabolic rate compared to WT mice, we predicted that *aNotch1* mice should be resistant to high-fat diet (HFD)-induced obesity. Indeed, *aNotch1* mice were leaner after being fed HFD for 4 weeks (**Fig. 3a**) even though their daily energy intake was similar to that of their WT littermates (**Fig. 3b**). In addition, the *aNotch1* mice retained better glucose tolerance and higher insulin sensitivity after HFD feeding compared to WT mice (**Fig. 3c**,**d**).

This observation prompted us to examine whether HFD activates Notch signaling in WT mice. After HFD feeding, the expression of *Lep*, a surrogate indicator of mature adipocytes and obesity, was increased 20-fold (**Fig. 3e**), confirming the obesogenic effect of HFD. Coincidentally, mRNA and protein expression of Notch receptors and targets was induced by HFD (**Fig. 3e**,**f**). These results together suggest that activation of Notch signaling is associated with, and inactivation of Notch conversely prevents, HFD-induced obesity.

Adipocyte-specific activation of Notch signaling inhibits browning and glucose metabolism

As a complementary approach to the knockout mouse models, we carried out gain-of-function studies using adiponectin *(Adipoq)-cre*/*Rosa*^{N1ICD} mice (henceforth called *Adipoq*/N1ICD). As expected, the adipose tissue of *Adipoq*/N1ICD mice had higher expression levels of N1ICD, *Hes1* and *Hey1* compared to that of WT mice (**Fig. 4a**). The *Adipoq*/N1ICD mice were slightly (~6%) heavier than their WT littermates even though they had similar food intake (**Supplementary Fig. 4a**,**b**).

Notably, the *Adipoq*/N1ICD mice had lower glucose tolerance and insulin sensitivity compared with WT littermates (**Fig. 4b**,**c**). In addition,

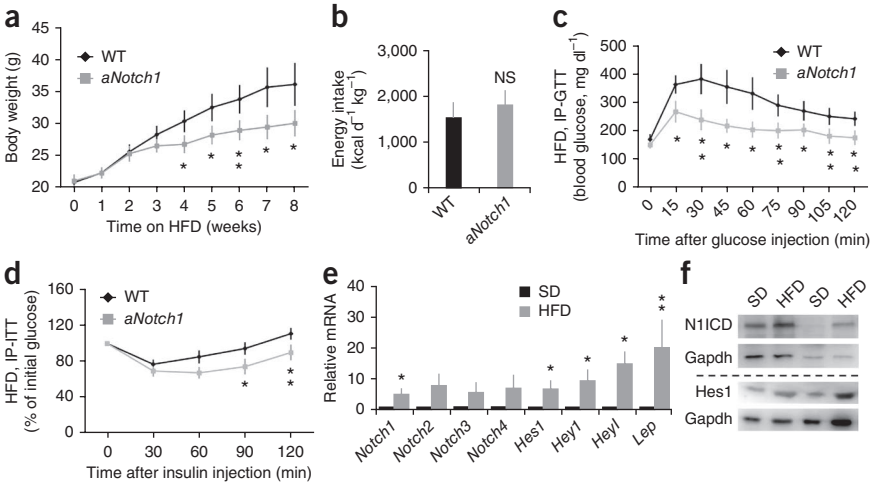

Figure 3 Resistance of *aNotch1* mice to HFD-induced obesity. (**a**,**b**) Growth curve (**a**) and energy intake assay (**b**, $n = 4$) of WT and *aNotch1* mice fed HFD. (**c**) Blood glucose concentrations during IP-GTT after glucose injection into fasted mice. (**d**) Blood glucose concentrations during IP-ITT after injecting insulin into fasted mice. (**e**) Gene expression assay of Notch receptors, Notch targets and *Lep* in WAT from mice fed standard diet (SD) or HFD for 3 weeks ($n = 8$). (**f**) Representative western blot ($n = 3$) for Notch activity of the sample treated as in **e**. $^*P < 0.05$, $^{**}P < 0.01$ (two-tailed Student's *t* test). NS, not significant. Data are shown as the means ± s.e.m. $n = 5$ pairs of mice unless otherwise indicated.

the metabolic rate and body temperature of *Adipoq*/N1ICD mice were also lower than those in WT mice (**Fig. 4d–g**) and were accompanied by lower expression levels of thermogenic and mitochondrial respiration-related genes in the IngWAT but not BAT (**Fig. 4h**,**i**). Furthermore, BAT from *Adipoq*/N1ICD mice accumulated more lipid droplets, and the size of the lipid droplets appeared larger than those in BAT from WT mice (**Fig. 4j**). Compared to the WT mice, the *Adipoq*/N1ICD mice were also less responsive to cold-induced browning, as manifested by a lower abundance of $Ucp1^+$ beige adipocytes and lower expression levels of Ucp1 and Pgc1-α proteins in IngWAT after being acclimated to 4 °C (**Supplementary Fig. 4c**,**d**). Thus, genetic activation of Notch signaling in adipocytes impairs body energy metabolism.

Notch signaling inhibits the expression of *Prdm16* and *Ppargc1a* in white adipocytes

To understand the cellular and molecular mechanisms through which Notch signaling regulates adipocytes, we first employed loss-of-function studies in cell culture. We cultured SVF preadipocytes from subcutaneous WAT of *Notch1*$^{flox/flox}$ mice. After transfection with a Cre plasmid, the expression of *Notch1* and its downstream target *Hes1* were reduced by more than 50% (**Fig. 5a**), which was accompanied by an upregulation of *Prdm16* and *Ppargc1a* expression (**Fig. 5a**). In parallel, we inhibited Notch signaling in white adipocytes from WT mice with the γ-secretase inhibitor DAPT. DAPT upregulated the expression of *Ucp1*, *Cidea*, *Prdm16* and *Ppargc1a* (**Fig. 5b** and **Supplementary Fig. 5a**,**b**). Similarly, adipocytes cultured from IngWAT of *aNotch1* mice expressed higher levels of *Ucp1*, *Ppargc1a* and *Prdm16* than adipocytes from WT mice (**Supplementary Fig. 5c**,**d**). Moreover, inguinal adipocytes from *aNotch1* mice exhibited higher O_2 consumption rate (OCR) than those from WT mice after stimulation with palmitate (**Supplementary Fig. 5e**). These results demonstrate that inhibition of Notch signaling enhances the expression of brown (beige) adipocyte-specific genes and the cellular respiration of white adipocytes in a cell-autonomous manner.

We also performed Notch gain-of-function studies by using SVF cells isolated from the subcutaneous WAT of *Rosa*^{N1ICD} mice and then transfecting them with GFP (control) or Cre plasmids. Compared to the control group, Cre-transfected SVF cells expressed higher levels of N1ICD, *Hes1* and *Hey1* but lower levels of *Prdm16* and *Ppargc1a*

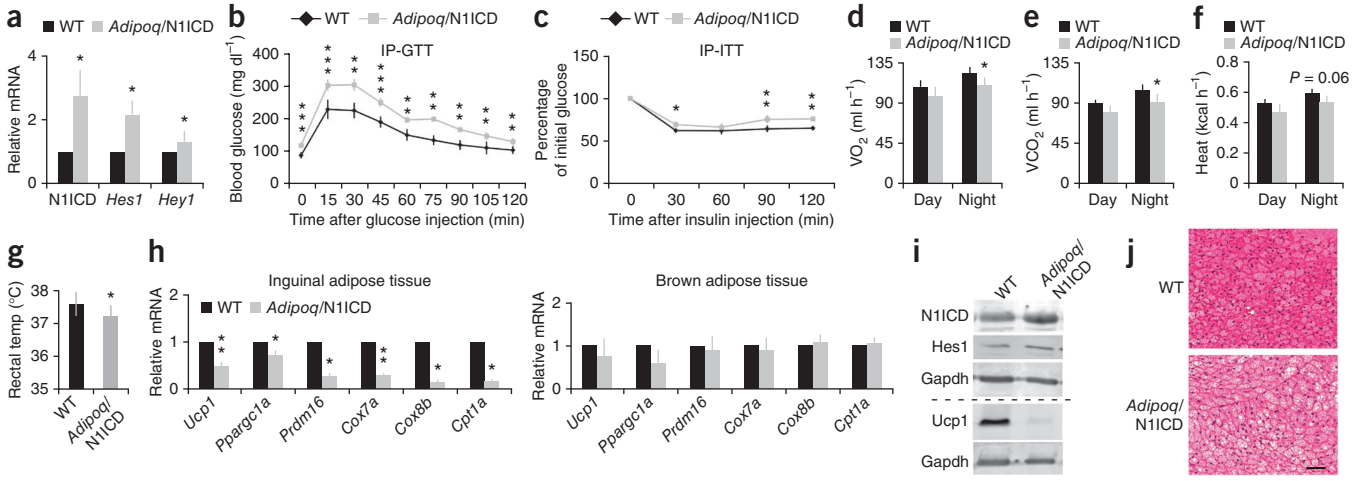

Figure 4 Activation of Notch1 in adipocytes inhibits browning and glucose metabolism. (**a**) Relative expression of N1ICD and its target genes in WAT. (**b**,**c**) Blood glucose concentrations during IP-GTT (**b**, $n = 6$) and IP-ITT (**c**) performed on 5- to 8-week-old WT and *Adipoq*/N1ICD mice. (**d**–**f**) O_2 consumption (**d**), CO_2 production (**e**) and heat production (**f**). (**g**) Rectal temperature ($n = 5$). (**h**) Relative expression of BAT and mitochondria marker genes in IngWAT (left) and BAT (right). (**i**) Representative western blot ($n = 3$) of IngWAT. (**j**) H&E staining of a BAT section. Scale bar, 50 μm. $^*P < 0.05$, $^{**}P < 0.01$, $^{***}P < 0.001$ (two-tailed Student's *t* test). Data are shown as the means ± s.e.m. $n = 4$ pairs of mice unless otherwise indicated.

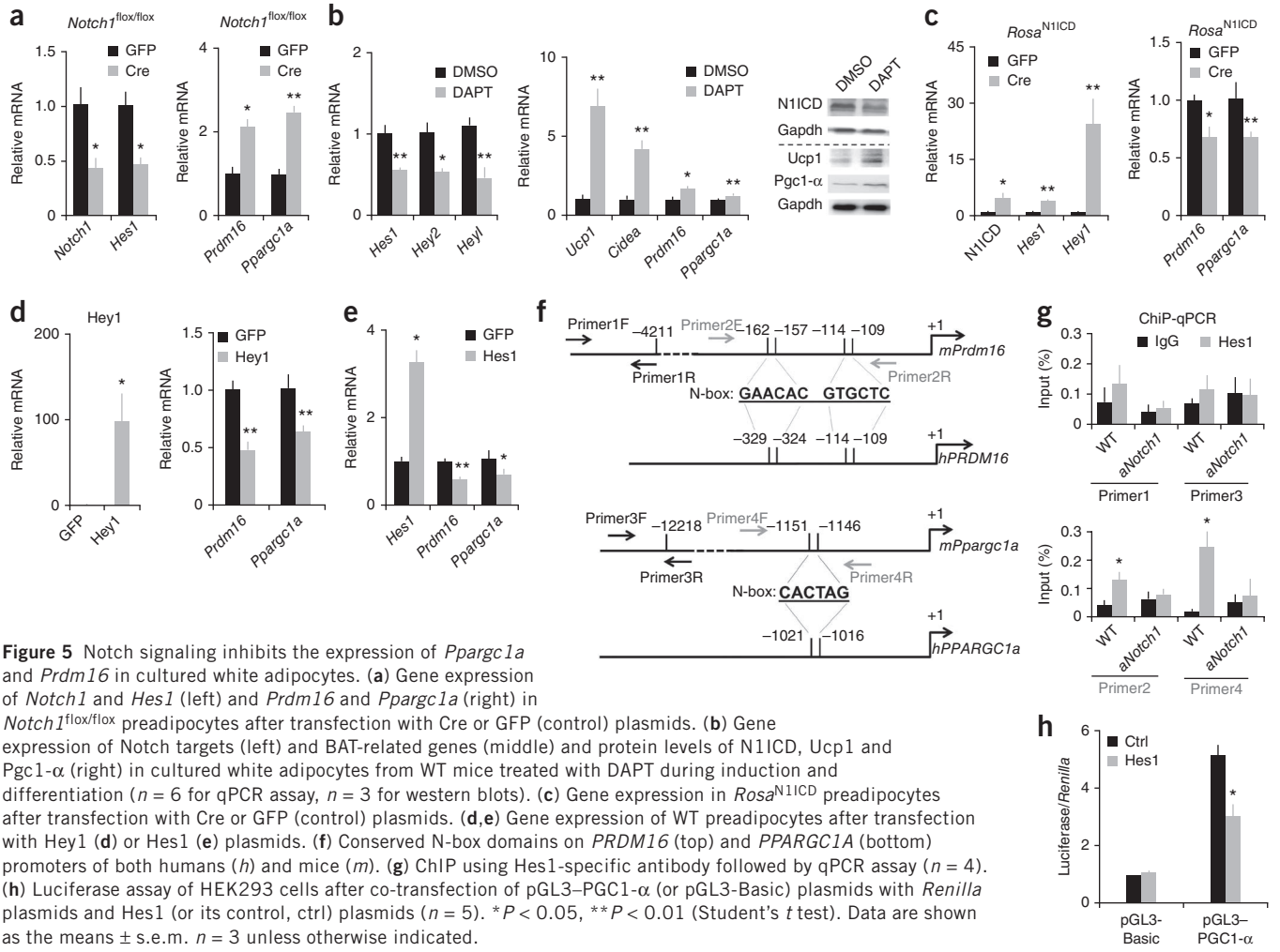

Figure 5 Notch signaling inhibits the expression of *Ppargc1a* and *Prdm16* in cultured white adipocytes. (**a**) Gene expression of *Notch1* and *Hes1* (left) and *Prdm16* and *Ppargc1a* (right) in *Notch1*$^{flox/flox}$ preadipocytes after transfection with Cre or GFP (control) plasmids. (**b**) Gene expression of Notch targets (left) and BAT-related genes (middle) and protein levels of N1ICD, Ucp1 and Pgc1-α (right) in cultured white adipocytes from WT mice treated with DAPT during induction and differentiation ($n = 6$ for qPCR assay, $n = 3$ for western blots). (**c**) Gene expression in *Rosa*^{N1ICD} preadipocytes after transfection with Cre or GFP (control) plasmids. (**d**,**e**) Gene expression of WT preadipocytes after transfection with Hey1 (**d**) or Hes1 (**e**) plasmids. (**f**) Conserved N-box domains on *PRDM16* (top) and *PPARGC1A* (bottom) promoters of both humans (*h*) and mice (*m*). (**g**) ChIP using Hes1-specific antibody followed by qPCR assay ($n = 4$). (**h**) Luciferase assay of HEK293 cells after co-transfection of pGL3–PGC1-α (or pGL3-Basic) plasmids with *Renilla* plasmids and Hes1 (or its control, ctrl) plasmids ($n = 5$). $^*P < 0.05$, $^{**}P < 0.01$ (Student's *t* test). Data are shown as the means ± s.e.m. $n = 3$ unless otherwise indicated.

(**Fig. 5c**). Overexpression of *Hey1* or *Hes1* alone in SVF cells of WT mice similarly led to lower levels of *Prdm16* and *Ppargc1a* as compared to the control (GFP) treatment (**Fig. 5d**,**e**). Together, activation of N1ICD or overexpressing Notch target genes suppressed the expression of the brown fat–associated genes *Prdm16* and *Ppargc1a*.

These results prompted us to ask whether the transcriptional repressor Hes1 can directly bind the promoter of *Prdm16* and *Ppargc1a*. Bioinformatics analysis identified consensus N-box (CACNAG) sites in the proximal promoter regions of mouse and human *PRDM16* and *PPARGC1A* (**Fig. 5f**). Chromatin immunoprecipitation (ChIP) using a Hes1-specific antibody followed by qPCR assay using primers flanking the N-box region showed that these predicted binding sites in the *Prdm16* and *Ppargc1a* promoter regions were enriched by 3- and 13-fold, respectively (**Fig. 5g**). However, enrichment of these regions was abolished in adipocytes from *aNotch1* mice (**Fig. 5g**). As a control, the Hes1-specific antibody failed to enrich random promoter regions that do not contain the N-box sequence (**Fig. 5g**), confirming the specificity of Hes1 binding to the N-box. Furthermore, Hes1 overexpression inhibited *Ppargc1a* promoter–driven luciferase reporter activity (**Fig. 5h**). These results suggest that the canonical Notch target Hes1 can bind directly to the promoters of *Prdm16* and *Ppargc1a* to repress their expression, thereby inhibiting brown (beige) gene programs.

Notch inhibition induces browning and ameliorates obesity in *Lep*^{ob} mice

To explore the therapeutic potential of targeting Notch signaling to improve glucose metabolism, we treated WT mice with a pharmacological inhibitor of Notch signaling. We injected littermate mice of similar body weight with dibenzazepine (DBZ), another γ-secretase inhibitor, or vehicle control for 5 days consecutively. Notably, DBZ-treated mice had better glucose tolerance and insulin sensitivity than control mice (**Supplementary Fig. 6a**,**b**). At the molecular level, DBZ treatment resulted in higher Ucp1 mRNA and protein expression in IngWAT and EpiWAT compared to vehicle treatment (**Supplementary Fig. 6c**,**d**). Adipocyte volume and number are positively correlated with leptin production[38], and we found lower *Lep* expression and less adiposity but a higher number of Ucp1$^+$ adipocytes in DBZ-treated mice than in control mice (**Supplementary Fig. 6e**,**f**). Hence, Notch inhibition reduced adiposity and improved glucose homeostasis in healthy mice.

To further investigate whether Notch inhibition ameliorates obesity under pathological conditions, we treated ob/ob mice deficient in *Lep* (*Lep*^{ob}) with DBZ. We grouped the mice randomly, and the groups showed no difference in body-weight gain before treatment (**Fig. 6a**). Notably, DBZ treatment attenuated the body-weight gain seen in the vehicle-treated control group without affecting energy intake (**Fig. 6a**,**b**). The body-weight differences were associated with smaller

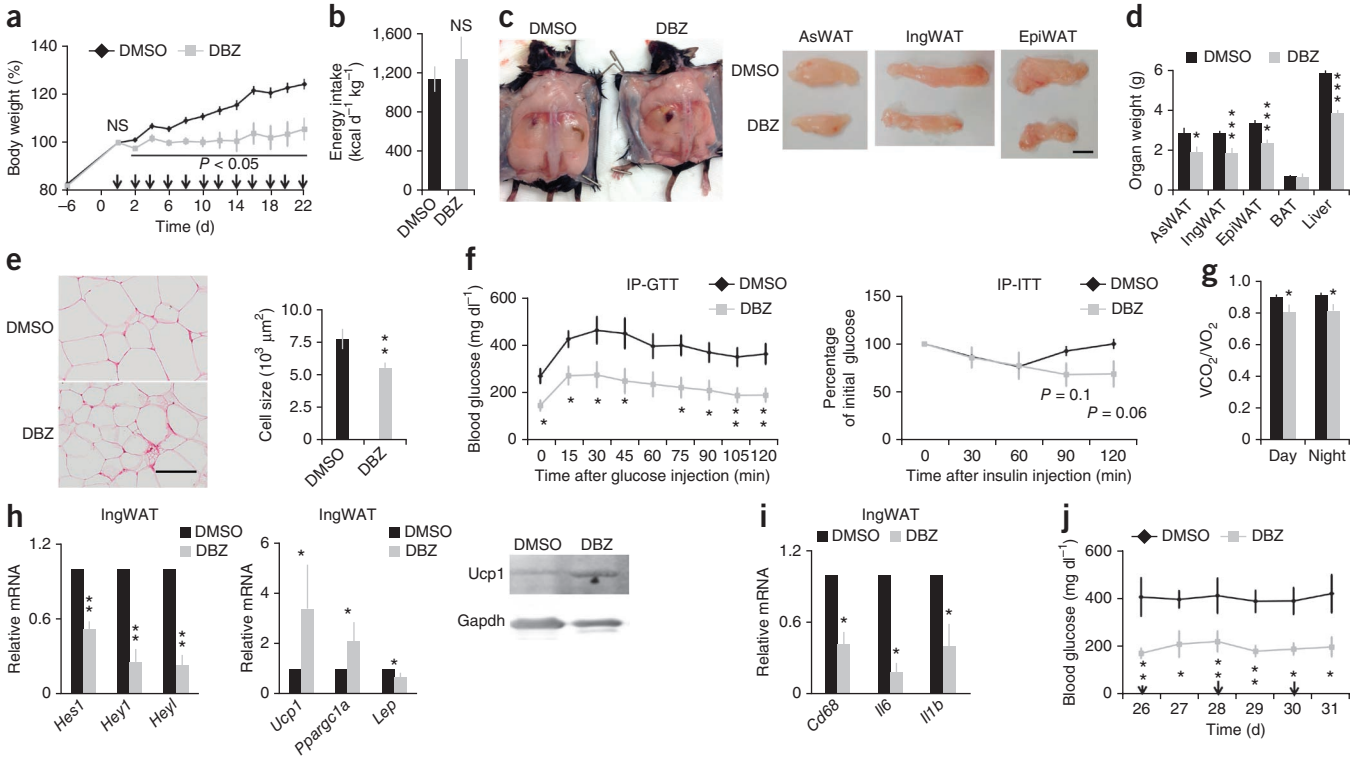

Figure 6 Inhibition of Notch in *Lep*-deficient obese mice (*Lep*^{ob}) ameliorates obesity and glucose metabolism. (**a**) Body weight ratio normalized to day 0. Arrows mark the doses of DMSO or DBZ injection. (**b**) Energy intake assay. (**c**) WAT images. Scale bar, 1 cm. (**d**) Tissue weight. (**e**) H&E staining of IngWAT (left; scale bar, 100 μm) and adipocyte size (right). (**f**) Plasma glucose measurements during IP-GTT (left) or IP-ITT (right). (**g**) Respiration exchange ratio of mice after treatment with DMSO or DBZ for 22 d. (**h**,**i**) Relative expression of Notch targets (**h** left), adipocyte genes (**h** middle), Ucp1 protein (**h** right, $n = 3$) and inflammation-related genes (**i**) in IngWAT. (**j**) Fed plasma glucose concentrations at the days shown. The arrows indicate DMSO or DBZ injection (starting from day 0, as shown in **a**). $^{*}P < 0.05$, $^{**}P < 0.01$, $^{***}P < 0.001$ (Student's *t* test). NS, not significant. Data are shown as the means ± s.e.m. $n = 5$.

size and less weight of various WAT depots in the DBZ-treated compared to vehicle-treated mice (**Fig. 6c–e** and **Supplementary Fig. 7a**,**b**). DBZ-treated mice also had lower liver weight and less hepatic lipid accumulation (**Fig. 6d** and **Supplementary Fig. 7a**), which are consistent with previous observations that Notch promotes lipogenesis in hepatocytes and liver steatosis[39]. In addition, glucose tolerance and insulin sensitivity were improved by DBZ treatment (**Fig. 6f**). Consistent with reduced adiposity, DBZ-treated mice showed a lower respiration exchange ratio compared with control mice (**Fig. 6g**), indicating that DBZ initiated a metabolic shift toward the utilization of fat as the energy source.

At the molecular level, DBZ inhibited the expression of the Notch targets *Hes1*, *Hey1* and *Heyl* as well as *Lep* (**Fig. 6h**) but upregulated the expression of *Ucp1* and *Ppargc1a* in WAT (**Fig. 6h**). DBZ also suppressed the expression of the inflammatory cytokines encoded by *Cd68*, *Il6* and *Il1b* (**Fig. 6i**) that are associated with obesity in humans[40]. At end of the experiment, fed blood glucose concentrations remained low in the absence of DBZ injection (**Fig. 6j**), suggesting a long-term beneficial effect of adipose browning on glucose metabolism. These results together provide strong evidence that the Notch signaling pathway can be pharmacologically targeted to prevent and treat obesity and improve glucose tolerance and insulin sensitivity.

DISCUSSION

Our study reveals a previously unrecognized yet critical role of Notch signaling in regulating the browning of adipose tissues and body insulin sensitivity. We have provided compelling genetic, physiological, metabolic, histological, cellular and molecular evidence to demonstrate that blockage of Notch signaling promotes the browning of WAT. Conversely, activation of Notch signaling represses the expression of genes critical for BAT biogenesis and is associated with whitening of BAT and poor insulin sensitivity. As Notch signaling is highly conserved in the animal kingdom, we anticipate that our results in mice will be applicable to humans, although future studies dissecting the role of Notch signaling in human adipose tissues will be imperative.

We used *aP2-cre* mice to drive the deletion of *Notch1* or *Rbpj* in adipose tissues. Although the *aP2-cre* expression domain falls predominantly in immature and mature adipocytes, leaky expression of this promoter has been reported in several other cell types[41–44]. Coincidently, Notch inhibition has been shown to improve insulin sensitivity through regulating liver glucose metabolism and attenuating atherosclerosis[45,46]. Even though we used a more adipocyte-restricted *Adipoq-cre* mouse model[47] to show that Notch activation conversely induces whitening of BAT and reduces glucose tolerance, we cannot exclude the possibility that Notch signaling in other cell types may have also contributed to the metabolic improvements of the *aNotch1* mice.

The white- to brown-fat transition involves a series of cellular processes, including increased Ucp1 expression, mitochondria production, lipolysis and β-oxidation. These features are all observed in the WAT but not BAT of Notch mutant mice. The differential responses of BAT and WAT to Notch signaling are perhaps due to the different

embryonic origins of these tissues, as well as cell type–specific gene regulatory programs. Of note, the higher Ucp1 level in white adipocytes from *aNotch1* mice was associated with enhanced uncoupled respiration and thermogenesis, which may have led to a higher core body temperature. However, as mammalian body temperature is controlled by the central nervous system, the subtle increases in core body temperature in *Notch* mutants suggest that Notch signaling may also have a role in central nervous system–mediated body temperature regulation. Alternatively, as both Notch signaling and core body temperature exhibit circadian rhythms (i.e., they oscillate during a day)[48,49], perturbations in Notch signaling may have altered the normal rhythm of core body temperature.

We used ChIP assay to demonstrate that the transcriptional co-repressor Hes1 binds directly to the promoter regions of *Ppargc1a* and *Prdm16*, whose expression is inhibited by Hes1 overexpression. Hey proteins can also inhibit the expression of Hes1 targets through dimerization with Hes1 (ref. 50). Consistent with this notion, we observed that overexpression of Hey1 also inhibited the transcription of *Ppargc1a* and *Prdm16*. In addition, NICD may recruit Gcn5 (also called Kat2a), a cofactor of the Rbpj transcription complex[51] and a major acetyltransferase of Pgc1-α, to repress its transcriptional activity[52]. Contradictory to our finding, Hes1 has been shown to positively regulate the expression of Prdm16 during mouse neurogenesis[53]. As Hes1 is a canonical transcriptional repressor, it probably acts through other mediators to upregulate Prdm16 indirectly in the neural system. These observations underscore the importance of cell context–dependent action of Notch signaling[54].

We found that HFD increased Notch activity in WAT, and *aNotch1* mutants were resistant to HFD-induced obesity. These results indicate that activation of Notch signaling is linked to the initiation and development of obesity. Our observation is in agreement with a recent study showing that a high-fat, high-cholesterol diet increases the expression of Dll4 (a Notch ligand) in the atheroma and fat tissue of *Ldlr*-deficient mice[46]. It is currently unclear how Notch signaling is activated at the onset of obesity. In addition, a recent study showed that excessive leptin production in mice with diet-induced obesity activates Notch signaling in metastatic breast cancer cells[55]. As we observed that inhibition of Notch reduced the expression of *Lep* in adipose tissues, it is possible that a positive feedback loop between Notch signaling and excessive leptin production together accelerates the development of obesity. Treating Lep^{ob} mice with γ-secretase inhibitor reduced body weight and ameliorated glucose metabolism, and such a drastic effect may be elicited not only by browning of white adipocytes but also through targeting of other important metabolic organs, including the liver and intestine, which directly regulate lipid metabolism and nutrient absorption, respectively[39,56]. Pharmacological approaches targeting adipose tissue specifically will clarify the direct contribution of adipose tissue to metabolic improvements after Notch inhibition.

One important future question is whether Notch signaling is involved in the commitment and specification of progenitors to become beige or classical white adipocytes. Several lines of evidence suggest that browning is an inherent capability that is restricted to a certain cell population that has a standby or predisposed machinery to respond to browning cues[19,57]. As Notch signaling is widely employed to control cell fate during development, it is important to examine how Notch regulates the cell fate specification of embryonic beige progenitors.

METHODS

Methods and any associated references are available in the online version of the paper.

Note: Any Supplementary Information and Source Data files are available in the online version of the paper.

ACKNOWLEDGMENTS

We thank T. Honjo (Kyoto University, Japan) for providing the $Rbpj^{flox/flox}$ mice; Dow AgroScience for providing Methocel E4M reagent; K. Ajuwon for providing access to the calorimetry facility; S. Koser and S. Donkin for assistance with luciferase assays; D. Zhou for Odyssey imaging facility support; T. Wiegand and C. Bain for assistance with histology; J. Wu and S. Hobaugh for maintaining mouse colonies; and members of the Kuang laboratory for comments. This work was partially supported by a grant from the US National Institutes of Health (R01AR060652 to S.K.).

AUTHOR CONTRIBUTIONS

P.B. and S.K. conceived the project, designed the experiments and prepared the manuscript. P.B., T.S., W.L., F.Y., X.Y., X.-R.L., J.W. and J.L. performed the experiments. N.C. provided reagents. P.B., T.S., W.L., X.L. and S.K. analyzed the data.

COMPETING FINANCIAL INTERESTS

The authors declare no competing financial interests.

1. Smith, R.E. Thermoregulatory and adaptive behavior of brown adipose tissue. *Science* **146**, 1686–1689 (1964).
2. Nedergaard, J. & Cannon, B. The changed metabolic world with human brown adipose tissue: therapeutic visions. *Cell Metab.* **11**, 268–272 (2010).
3. Rosen, E.D. & Spiegelman, B.M. Adipocytes as regulators of energy balance and glucose homeostasis. *Nature* **444**, 847–853 (2006).
4. Tran, T.T. & Kahn, C.R. Transplantation of adipose tissue and stem cells: role in metabolism and disease. *Nat. Rev. Endocrinol.* **6**, 195–213 (2010).
5. van Marken Lichtenbelt, W.D. *et al.* Cold-activated brown adipose tissue in healthy men. *N. Engl. J. Med.* **360**, 1500–1508 (2009).
6. Saito, M. *et al.* High incidence of metabolically active brown adipose tissue in healthy adult humans: effects of cold exposure and adiposity. *Diabetes* **58**, 1526–1531 (2009).
7. Virtanen, K.A. *et al.* Functional brown adipose tissue in healthy adults. *N. Engl. J. Med.* **360**, 1518–1525 (2009).
8. Cypess, A.M. *et al.* Identification and importance of brown adipose tissue in adult humans. *N. Engl. J. Med.* **360**, 1509–1517 (2009).
9. Zingaretti, M.C. *et al.* The presence of UCP1 demonstrates that metabolically active adipose tissue in the neck of adult humans truly represents brown adipose tissue. *FASEB J.* **23**, 3113–3120 (2009).
10. Cypess, A.M. *et al.* Anatomical localization, gene expression profiling and functional characterization of adult human neck brown fat. *Nat. Med.* **19**, 635–639 (2013).
11. Jespersen, N.Z. *et al.* A classical brown adipose tissue mRNA signature partly overlaps with brite in the supraclavicular region of adult humans. *Cell Metab.* **17**, 798–805 (2013).
12. Lidell, M.E. *et al.* Evidence for two types of brown adipose tissue in humans. *Nat. Med.* **19**, 631–634 (2013).
13. Schulz, T.J. *et al.* Brown-fat paucity due to impaired BMP signalling induces compensatory browning of white fat. *Nature* **495**, 379–383 (2013).
14. Fisher, F.M. *et al.* FGF21 regulates PGC-1α and browning of white adipose tissues in adaptive thermogenesis. *Genes Dev.* **26**, 271–281 (2012).
15. Ohno, H., Shinoda, K., Spiegelman, B.M. & Kajimura, S. PPARγ agonists induce a white-to-brown fat conversion through stabilization of PRDM16 protein. *Cell Metab.* **15**, 395–404 (2012).
16. Seale, P. *et al.* Prdm16 determines the thermogenic program of subcutaneous white adipose tissue in mice. *J. Clin. Invest.* **121**, 96–105 (2011).
17. Frontini, A. *et al.* White-to-brown transdifferentiation of omental adipocytes in patients affected by pheochromocytoma. *Biochim. Biophys. Acta* **1831**, 950–959 (2013).
18. Wu, J. *et al.* Beige adipocytes are a distinct type of thermogenic fat cell in mouse and human. *Cell* **150**, 366–376 (2012).
19. Wang, Q.A., Tao, C., Gupta, R.K. & Scherer, P.E. Tracking adipogenesis during white adipose tissue development, expansion and regeneration. *Nat. Med.* **19**, 1338–1344 (2013).
20. Rosenwald, M., Perdikari, A., Rulicke, T. & Wolfrum, C. Bi-directional interconversion of brite and white adipocytes. *Nat. Cell Biol.* **15**, 659–667 (2013).
21. Ye, L. *et al.* Fat cells directly sense temperature to activate thermogenesis. *Proc. Natl. Acad. Sci. USA* **110**, 12480–12485 (2013).

22. Cao, L. *et al.* White to brown fat phenotypic switch induced by genetic and environmental activation of a hypothalamic-adipocyte axis. *Cell Metab.* **14**, 324–338 (2011).
23. Shabalina, I.G. *et al.* UCP1 in brite/beige adipose tissue mitochondria is functionally thermogenic. *Cell Reports* **5**, 1196–1203 (2013).
24. Pfannenberg, C. *et al.* Impact of age on the relationships of brown adipose tissue with sex and adiposity in humans. *Diabetes* **59**, 1789–1793 (2010).
25. Ouellet, V. *et al.* Outdoor temperature, age, sex, body mass index, and diabetic status determine the prevalence, mass, and glucose-uptake activity of 18F-FDG–detected BAT in humans. *J. Clin. Endocrinol. Metab.* **96**, 192–199 (2011).
26. Schroeter, E.H., Kisslinger, J.A. & Kopan, R. Notch-1 signalling requires ligand-induced proteolytic release of intracellular domain. *Nature* **393**, 382–386 (1998).
27. Ross, D.A., Rao, P.K. & Kadesch, T. Dual roles for the Notch target gene Hes-1 in the differentiation of 3T3–L1 preadipocytes. *Mol. Cell. Biol.* **24**, 3505–3513 (2004).
28. Garcés, C. *et al.* Notch-1 controls the expression of fatty acid–activated transcription factors and is required for adipogenesis. *J. Biol. Chem.* **272**, 29729–29734 (1997).
29. Lai, P.Y., Tsai, C.B. & Tseng, M.J. Active form Notch4 promotes the proliferation and differentiation of 3T3–L1 preadipocytes. *Biochem. Biophys. Res. Commun.* **430**, 1132–1139 (2013).
30. Urs, S. *et al.* Effect of soluble Jagged1-mediated inhibition of Notch signaling on proliferation and differentiation of an adipocyte progenitor cell model. *Adipocyte* **1**, 46–57 (2012).
31. Vujovic, S., Henderson, S.R., Flanagan, A.M. & Clements, M.O. Inhibition of γ-secretases alters both proliferation and differentiation of mesenchymal stem cells. *Cell Prolif.* **40**, 185–195 (2007).
32. Osathanon, T., Subbalekha, K., Sastravaha, P. & Pavasant, P. Notch signalling inhibits the adipogenic differentiation of single-cell–derived mesenchymal stem cell clones isolated from human adipose tissue. *Cell Biol. Int.* **36**, 1161–1170 (2012).
33. Huang, Y. *et al.* γ-secretase inhibitor induces adipogenesis of adipose-derived stem cells by regulation of Notch and PPAR-γ. *Cell Prolif.* **43**, 147–156 (2010).
34. Nichols, A.M. *et al.* Notch pathway is dispensable for adipocyte specification. *Genesis* **40**, 40–44 (2004).
35. Stanford, K.I. *et al.* Brown adipose tissue regulates glucose homeostasis and insulin sensitivity. *J. Clin. Invest.* **123**, 215–223 (2013).
36. Orava, J. *et al.* Different metabolic responses of human brown adipose tissue to activation by cold and insulin. *Cell Metab.* **14**, 272–279 (2011).
37. Cannon, B. & Nedergaard, J. Nonshivering thermogenesis and its adequate measurement in metabolic studies. *J. Exp. Biol.* **214**, 242–253 (2011).
38. Rosenbaum, M. & Leibel, R.L. The role of leptin in human physiology. *N. Engl. J. Med.* **341**, 913–915 (1999).
39. Pajvani, U.B. *et al.* Inhibition of Notch uncouples Akt activation from hepatic lipid accumulation by decreasing mTorc1 stability. *Nat. Med.* **19**, 1054–1060 (2013).
40. Weisberg, S.P. *et al.* Obesity is associated with macrophage accumulation in adipose tissue. *J. Clin. Invest.* **112**, 1796–1808 (2003).
41. Martens, K., Bottelbergs, A. & Baes, M. Ectopic recombination in the central and peripheral nervous system by aP2/FABP4-Cre mice: implications for metabolism research. *FEBS Lett.* **584**, 1054–1058 (2010).
42. Urs, S., Harrington, A., Liaw, L. & Small, D. Selective expression of an aP2/fatty acid binding protein 4–Cre transgene in non-adipogenic tissues during embryonic development. *Transgenic Res.* **15**, 647–653 (2006).
43. Mullican, S.E. *et al.* A novel adipose-specific gene deletion model demonstrates potential pitfalls of existing methods. *Mol. Endocrinol.* **27**, 127–134 (2013).
44. Lee, K.Y. *et al.* Lessons on conditional gene targeting in mouse adipose tissue. *Diabetes* **62**, 864–874 (2013).
45. Pajvani, U.B. *et al.* Inhibition of Notch signaling ameliorates insulin resistance in a FoxO1-dependent manner. *Nat. Med.* **17**, 961–967 (2011).
46. Fukuda, D. *et al.* Notch ligand δ-like 4 blockade attenuates atherosclerosis and metabolic disorders. *Proc. Natl. Acad. Sci. USA* **109**, E1868–E1877 (2012).
47. Eguchi, J. *et al.* Transcriptional control of adipose lipid handling by IRF4. *Cell Metab.* **13**, 249–259 (2011).
48. Gerhart-Hines, Z. *et al.* The nuclear receptor Rev-erbα controls circadian thermogenic plasticity. *Nature* **503**, 410–413 (2013).
49. Bray, S.J. Notch signalling: a simple pathway becomes complex. *Nat. Rev. Mol. Cell Biol.* **7**, 678–689 (2006).
50. Iso, T. *et al.* HERP, a novel heterodimer partner of HES/E^{spl} in Notch signaling. *Mol. Cell. Biol.* **21**, 6080–6089 (2001).
51. Kurooka, H. & Honjo, T. Functional interaction between the mouse Notch1 intracellular region and histone acetyltransferases PCAF and GCN5. *J. Biol. Chem.* **275**, 17211–17220 (2000).
52. Lerin, C. *et al.* GCN5 acetyltransferase complex controls glucose metabolism through transcriptional repression of PGC-1α. *Cell Metab.* **3**, 429–438 (2006).
53. Kinameri, E. *et al.* Prdm proto-oncogene transcription factor family expression and interaction with the Notch-Hes pathway in mouse neurogenesis. *PLoS ONE* **3**, e3859 (2008).
54. Schwanbeck, R., Martini, S., Bernoth, K. & Just, U. The Notch signaling pathway: molecular basis of cell context dependency. *Eur. J. Cell Biol.* **90**, 572–581 (2011).
55. Battle, M. *et al.* Obesity induced a leptin-Notch signaling axis in breast cancer. *Int. J. Cancer* **134**, 1605–1616 (2014).
56. Zecchini, V., Domaschenz, R., Winton, D. & Jones, P. Notch signaling regulates the differentiation of post-mitotic intestinal epithelial cells. *Genes Dev.* **19**, 1686–1691 (2005).
57. Liu, W. *et al.* A heterogeneous lineage origin underlies the phenotypic and molecular differences of white and beige adipocytes. *J. Cell Sci.* **126**, 3527–3532 (2013).

ONLINE METHODS

Animals. All procedures involving mice were performed in accordance with Purdue University's Animal Care and Use Committee. The *Rbpj*$^{flox/flox}$ mouse was previously described[58] and kindly provided by T. Honjo (Kyoto University). Other mice used were purchased from Jackson lab as follows: *Notch1*$^{flox/flox}$ (stock 007181)[59], *aP2-cre* (stock 005069)[60], *adiponectin-cre* (stock 010803)[47], *Lep*^{ob} (stock 000632)[61], *Rosa*^{N1ICD} (stock 008159)[62] and *Rosa*^{eYFP} (stock 007920). Mice were in a C57BL/6J or mixed background and housed in the animal facility with free access to water and standard rodent chow food or HFD (TD.06414 Harlan). Male and female mice 2–4 months of age were used unless otherwise indicated.

Energy intake assay was calculated by measuring food consumption, and data are presented as the food weight multipled by its energy content and then normalized to the body weight of the mice and number of days.

Indirect calorimetry study. Oxygen consumption (VO_2), carbon dioxide production (VCO_2), respiratory exchange ratios (VCO_2/VO_2) and heat production were measured using an indirect calorimetry system (Oxymax, Columbus Instruments) installed under a constant environmental temperature (22 °C) and a 12-h light, 12-h dark cycle. Mice in each chamber had free access to food and water.

Rectal temperature measurement. A digital thermometer (ETI model MicroTherma 2) was used in combination with a copper thermocouple probe (Type T). The probe was inserted 2 cm or 1.6 cm into the anal ducts of male and female adult mice (2–4 months old), respectively. Temperature was measured at around 4 p.m.

Glucose uptake by WAT explants. Mice were fasted for 20 h (from 6 p.m. to 2 p.m. of the next day). Intact inguinal adipose tissue was carefully dissected to be free of visible connective tissue and immediately placed in ice-cold PBS for 5 min. WAT explants were then transferred to 37 °C prewarmed DMEM (glucose free) supplemented with 10 nM insulin for 30 min at 37 °C with 5% CO_2. For glucose consumption measurements, WAT was then transferred to 24 wells with 1 ml DMEM supplemented with 100 nM insulin and 1,000 mg l^{-1} glucose per well and incubated at 37 °C with 5% CO_2. Media (50 µl) were collected for glucose measurements at 60 and 120 min. Glucose consumption was calculated based on the glucose concentration of the medium collected and measured with a glucose test strip (Accu-Check Active, Roche) read by a glucometer (Accu-Check Active, Roche). The readings were calibrated based on a standard curve plotted using a gradient of known concentrations of glucose in DMEM ($R^2 > 0.99$).

DBZ treatment. DBZ was purchased from TOCRIS Bioscience (catalog number 4489) and used according to previous studies[45,63]. DBZ was dissolved in DMSO at a 100 mM concentration. After use, the stock was suspended at a 1:100 dilution in a solution containing 0.5% Methocel E4M (wt/vol; Dow Chemical) and 0.1% Tween-80 (wt/vol; Sigma) in H_2O. This working solution was mixed by vortex and sonication for 1 min each and injected intraperitoneally (i.p.) at a dosage of 10 µmol DBZ per kg body weight. Control groups were injected with equal volumes of DMSO diluted in the E4M and Tween-80 solution. Control and DBZ treatment groups were randomly determined. To test the effect of DBZ on genetically induced obesity, ob/ob (*Lep*^{ob}) mice (6 weeks old, male) were treated every other day for 1 month.

Blood glucose measurements. Five microliters of blood collected from the tail vein was dropped onto a glucose test strip (Accu-Check Active, Roche) and measured by a glucometer (Accu-Check Active, Roche). For glucose tolerance tests, mice were given i.p. injection of 100 mg ml^{-1} D-glucose (2 g kg^{-1} body weight for standard diet, 1 g kg^{-1} for HFD and 0.5 g kg^{-1} for *Lep*^{ob}) after overnight fasting, and tail blood glucose concentrations were monitored. For insulin tolerance tests, mice were fasted for 4 h before i.p. administration of human insulin (Santa Cruz) (0.75 U kg^{-1} body weight), and tail blood glucose concentrations were monitored. For both GTT and ITT, each mouse was singly caged with blinded cage number and random orders.

FACS and immunostaining. SVF cells were isolated from the inguinal WAT of 2-month-old WT mice fed a standard chow diet. To examine subpopulations of macrophage cells in the SVF, cells were sorted based on CD11b and F4/80 staining of SVF cells. For immunostaining, the digested SVF cells were cultured overnight, and attached cells were stained for CD68 (ab955).

Primary adipocyte culture, transfection and chemical treatment. SVF cells were isolated from subcutaneous WAT unless otherwise stated. Adipose tissue was minced and digested with 1.5 mg ml^{-1} collagenase at 37 °C for 1.5–2 h. The digestions were stopped with DMEM containing 10% FBS, filtered through 100-µm filters and centrifuged at 450*g* for 5 min. SVF cells were seeded and cultured in growth medium containing DMEM, 20% FBS and 1% penicillin/streptomycin at 37 °C with 5% CO_2 for 3 d. At confluence, the cells were collected and electroporated using a Neon transfection system (Invitrogen). Briefly, 10^5 cells were suspended in 10 µl electroporation buffer, including 2.5 µg plasmids, and electroporated (1,100 V, 10 ms, three times) using a 10-µl tip. After electroporation, the cells were seeded and cultured in six-well plates. All plasmids used were cloned as described[64]. Preadipocytes were induced to differentiate with induction medium containing DMEM, 10% FBS, 2.85 µM insulin, 0.3 µM dexamethasone (Sigma) and 0.63 mM 3-isobutyl-methylxanthine (Cayman Chemical) for 4 d and then spent 4 days in differentiation medium containing DMEM, 200 nM insulin and 10 nM T3 until the adipocytes matured. During the induction and differentiation, cells were treated with 10 µM DAPT (N-[N-(3,5-difluorophenacetyl)-1-alanyl]-S-phenylglycine t-butyl ester) (Cayman Chemical).

Adipocyte OCR measurement. Primary SVF cells from inguinal WAT were isolated and cultured for 3 d before being plated in XF cell culture microplates (Seahorse Bioscience). SVF cells (10,000 cells) were seeded in each well, and each sample had eight replicates. After 6 d of differentiation, cultured adipocytes were washed twice and pre-incubated in XF medium for 1–2 h at room temperature. The OCR was measured by the XF extracellular flux analyzer (Seahorse Biosciences). The chemicals (final concentration: 0.2 mM palmitate, 34 µM BSA and 2 µM Rotenone) were preloaded into cartridges and injected into XF wells in succession. OCR was calculated as a function of time (picomoles per minute).

Total RNA extraction, cDNA synthesis and real-time PCR. Total RNA was extracted from cells or tissues using TRIzol reagent according to the manufacturer's instructions. RNA was treated with RNase-free DNase I to remove contaminating genomic DNA. The purity and concentration of the total RNA were determined by a spectrophotometer (Nanodrop 2000c, Thermo Fisher) at 260 and 280 nm. The ratios of absorption (260 nm/280 nm) of all samples were between 1.8 and 2.0. Then 5 µg of total RNA was reverse transcribed using random primers with M-MLV reverse transcriptase (Invitrogen). Real-time PCR was carried out in a Roche Light Cycler 480 PCR System with SYBR Green Master Mix (Roche) and gene-specific primers as previously described[64,65]. The $2^{-\Delta\Delta Ct}$ method was used to analyze the relative changes in each gene's expression normalized against 18S rRNA expression.

Protein extraction and western blot analysis. Protein was isolated from cells or tissues using RIPA buffer containing 50 mM Tris-HCl (pH 8.0), 150 mM NaCl, 1% NP-40, 0.5% sodium deoxycholate and 0.1% SDS. Protein concentrations were determined using Pierce BCA Protein Assay Reagent (Pierce Biotechnology). Proteins were separated by SDS-PAGE, transferred to a polyvinylidene fluoride (PVDF) membrane (Millipore Corporation), blocked in 5% fat-free milk for 1 h at room temperature and then incubated with primary antibodies in 5% milk overnight at 4 °C. The UCP1 (ab23841), N1ICD (ab8925) and Hes1 (ab71559) antibodies were from Abcam, and the PGC1-α (sc-13067), GAPDH (sc-32233) and actin (sc-130656) antibodies were from Santa Cruz Biotechnology, and all were diluted 1:3,000. The horseradish peroxidase (HRP)-conjugated secondary antibody (anti-rabbit IgG, 111-035-003 or anti-mouse IgG; 115-035-003, Jackson ImmunoResearch) was diluted 1:5,000. Immunodetection was performed using enhanced chemiluminescence western blotting substrate (Pierce Biotechnology) and detected with a Gel Logic 2200 imaging system (Carestream). Alternatively, the membrane was incubated with an infrared secondary antibody (Alexa Fluor 790 goat anti-mouse IgG, A11357; Alexa Fluor 680 goat anti-rabbit IgG, A21109; Life Technologies, USA) diluted 1:10,000, and the signals were detected by using the Odyssey infrared image scanning system. Results shown in the figures are representative results from at least three independent experiments.

H&E and immunohistochemistry staining. Adipose tissues were fixed in 10% formalin for 24 h at room temperature. Then the tissues were embedded into paraffin and cut into 4-μm thick slices, deparaffinized and rehydrated using xylene, ethanol and water by standard methods. For antigen retrieval, slides were submerged in 0.01 M sodium citrate (pH 6.0) and heated to 96 °C for 20 min in a laboratory microwave (PELCO). Immunohistochemistry was performed on a Dako Autostainer (Dako, Carpinteria, CA). Slides were incubated with 3% hydrogen peroxide and 2.5% normal horse serum (S-2012, Vector), followed by incubation with rabbit polyclonal anti-UCP1 primary antibody diluted 1:200 in 2.5% normal horse serum (Vector, S-2012) for 60 min. Signals were detected with an anti-rabbit IgG Polymer Detection Kit (MP-7401, Vector). Labeling was visualized with 3,3′-diaminobenzidine (DAB) as the chromogen (SK-4105, Vector). Slides were counterstained with Harris hematoxylin (EK Industries, Joliet, IL), and whole-slide digital images were collected at 20× magnification with an Aperio Scan Scope slide scanner (Aperio, Vista, CA). Images shown are representative results of at least three biological replicates. Scanned images of H&E staining were analyzed by Photoshop CS3 to calculate cell numbers. Average adipocyte size was calculated as the image area divided by the cell number.

ChIP and genomic DNA recombination assay. Cultured inguinal adipocytes of both WT and mutant mice were crosslinked with 1% formaldehyde in DMEM for 10 min at room temperature followed by the addition of 125 mM glycine for 5 min at room temperature, after which cells were washed once with ice-cold PBS and scraped into SDS lysis buffer. The cells were further sonicated and diluted for immunoprecipitation with the indicated antibodies. The immunoprecipitates were eluted and reverse crosslinked overnight at 65 °C. DNA fragments were purified using the Cycle Pure kit (Omega Bio-Tek), and qPCR was performed with the primers listed in **Supplementary Table 1**. Genomic DNA was extracted from adipose tissue and amplified with the primers[66,67] listed in **Supplementary Table 1**.

Luciferase assay. HEK293A cells were seeded into 12-well plates 1 d before Lipofectamine 2000–mediated transfection. The PGC1-α promoter luciferase plasmid was purchased from Addgene and generated by Handschin *et al.*[68]. For transfection of each well, 100 ng *Renilla* plasmid, 400 ng pGL3-Basic (or pGL3–PGC1-α) and 600 ng Hes1 plasmid (or its blank control plasmid) were co-transfected following the manufacture's instructions. Cells were harvested 36 h after transfection and analyzed with the Dual-Luciferase Reporter Assay System (Promega).

Statistical analyses. Trial experiments or experiments done previously were used to determine sample size with adequate statistical power. Measurement values that were beyond the boundary determined by the interquartile range were considered as outliers and were excluded from statistical analyses. All analyses were conducted with Student's *t* test with a two-tail distribution. Comparisons with P values <0.05 were considered significant. The researchers involved in the study were not completely blinded during sample obtainment or data analysis.

58. Han, H. *et al.* Inducible gene knockout of transcription factor recombination signal binding protein-J reveals its essential role in T versus B lineage decision. *Int. Immunol.* **14**, 637–645 (2002).
59. Yang, X. *et al.* Notch activation induces apoptosis in neural progenitor cells through a p53-dependent pathway. *Dev. Biol.* **269**, 81–94 (2004).
60. He, W. *et al.* Adipose-specific peroxisome proliferator–activated receptor γ knockout causes insulin resistance in fat and liver but not in muscle. *Proc. Natl. Acad. Sci. USA* **100**, 15712–15717 (2003).
61. Coleman, D.L. & Hummel, K.P. The influence of genetic background on the expression of the obese (Ob) gene in the mouse. *Diabetologia* **9**, 287–293 (1973).
62. Murtaugh, L.C., Stanger, B.Z., Kwan, K.M. & Melton, D.A. Notch signaling controls multiple steps of pancreatic differentiation. *Proc. Natl. Acad. Sci. USA* **100**, 14920–14925 (2003).
63. Milano, J. *et al.* Modulation of notch processing by γ-secretase inhibitors causes intestinal goblet cell metaplasia and induction of genes known to specify gut secretory lineage differentiation. *Toxicol. Sci.* **82**, 341–358 (2004).
64. Wen, Y. *et al.* Constitutive Notch activation upregulates Pax7 and promotes the self-renewal of skeletal muscle satellite cells. *Mol. Cell. Biol.* **32**, 2300–2311 (2012).
65. Shan, T., Liang, X., Bi, P. & Kuang, S. Myostatin knockout drives browning of white adipose tissue through activating the AMPK-PGC1α-Fndc5 pathway in muscle. *FASEB J.* **27**, 1981–1989 (2013).
66. Demehri, S., Turkoz, A. & Kopan, R. Epidermal Notch1 loss promotes skin tumorigenesis by impacting the stromal microenvironment. *Cancer Cell* **16**, 55–66 (2009).
67. Gao, J. *et al.* Hedgehog signaling is dispensable for adult hematopoietic stem cell function. *Cell Stem Cell* **4**, 548–558 (2009).
68. Handschin, C., Rhee, J., Lin, J., Tarr, P.T. & Spiegelman, B.M. An autoregulatory loop controls peroxisome proliferator–activated receptor γ coactivator 1α expression in muscle. *Proc. Natl. Acad. Sci. USA* **100**, 7111–7116 (2003).

doi:10.1038/nm.3615